Local atomic structure of superconducting $FeSe_{1-x}Te_x$

Despina Louca,[1] K. Horigane,[2] A. Llobet,[3] R. Arita,[4,5] S. Ji,[1] N. Katayama,[1] S. Konbu,[4] K. Nakamura,[4,5] T.-Y. Koo,[6] P. Tong,[1] and K. Yamada[3]

[1]*Department of Physics, University of Virginia, Charlottesville, Virginia 22904, USA*

[2]*WPI Advanced Institute for Materials Research, Tohoku University, Katahira 2-1-1, Aoba, Sendai 980-8577, Japan*

[3]*Los Alamos National Laboratory, MS H805, Los Alamos, New Mexico 87545, USA*

[4]*Department of Applied Physics, University of Tokyo, Hongo, Tokyo 113-8656, Japan*

[5]*JST, TRIP, Sanbancho, Chiyoda, Tokyo 102-0075, Japan*

[6]*Pohang Accelerator Laboratory, Pohang University of Science and Technology, Pohang 790-784, Korea*

(Received 21 January 2010; revised manuscript received 31 March 2010; published 26 April 2010)

The isovalent substitution of Te for Se in the superconducting α-FeSe raises T_C where the average chalcogen–Fe bond angle decreases and the chalcogen-Fe distance increases. Locally, *however*, the Se and Te ions do not share the same site and have two distinct z coordinates, in contrast to what is presumed in the $P4/nmm$ symmetry. The local bond angle between the chalcogens and Fe increases with the substitution, consistent with the rise in T_C, the Fe–Te bonds become shorter than in the binary FeTe, while the Fe–Se bonds stay the same as in the binary. *Ab initio* calculations based on spin density functional theory yielded an optimized structure with distinct z coordinates for Se and Te, in addition to a stronger hybridization of Te with Fe.

DOI: 10.1103/PhysRevB.81.134524 PACS number(s): 74.70.Xa, 61.05.F−, 74.62.Dh, 74.20.Pq

I. INTRODUCTION

Magnetic fluctuations,[1,2] unconventional electron-phonon coupling,[3] and direct pairing interactions[4] are key elements in understanding the superconducting mechanism of the Fe-based pnictides.[5] Although several Fe systems with radically different compositions have been discovered thus far that exhibit superconductivity, their crystal structures share one common feature, namely, they consist of Fe tetrahedra coordinated by As/*P* or Se/Te. The calculations of electronic structures and magnetic properties[6–8] point to an unusual sensitivity of the bond lengths between ions as well as the bond angles, and their precise nature can be determined via the local atomic structure.

The ground state properties of the iron pnictides are quite perplexing[9] and uniquely different from those of copper oxides. For instance, charge doping is not vital to enhance T_C,[10] magnetic ion doping does not suppress T_C (Ref. 11) and magnetic fluctuations may persist in the superconducting phase such as in $FeSe_{1-x}Te_x$ (Refs. 9, 12, and 13) or even increase with T_C as reported in FeSe.[14] The nature of the superconducting gap is *s*-wave-like[15] but if an electron-phonon coupling mechanism is assumed, calculations[6,8] showed that it is not possible to obtain as high a T_C as it has been experimentally observed. This suggests that the Fe-pnictides are not BCS type superconductors. On the other hand, the observations of an isotope effect[3] and phonon anomalies[16] implicate the lattice. Furthermore, in the Fe-Se-Te system, with the structure shown in Fig. 1(a), T_C reaches a maximum by changing the ionic size from Se to Te without doping of excess charge while pressure enhancement of T_C (Refs. 17 and 18) directly implicates the crystal structure in the mechanism of superconductivity. Thus, it can be concluded that the Fe band structure is unique due to its particular ligand environment that can in turn be probed via the local atomic structure. This should be a key component to determining the degree of hybridization of the Fe orbitals with their surrounding ligand ions that in turn affects electron itinerancy,[19] the magnitude of the local moment and superconductivity.

Our results from the neutron pair density function (PDF) analysis point to a direct correlation of the local coordinates to T_C in the binary $FeSe_{1-x}Te_x$. The isovalent substitution of the nominally larger Te ion for Se increases T_C (Ref. 10) in comparison to α-FeSe (Refs. 20–22) with no additional carriers while, on average, the chalcogen–Fe bond angle, α, decreases and the bond length increases. However, we find that: (a) the local symmetry is lower than the average tetragonal $P4/nmm$ crystal symmetry because the Se and Te ions do not share the same site, leading to two distinct z coordinates that exhibit two types of bond angles and two types of bond lengths with Fe. Such modulations of the ionic lattice can change the distribution of valence electrons;[23] (b) the local bond angle, α, indeed increases with the substitution, in contrast to what is suggested from the average structure, which is in line with the finding in other arsenic superconductors that show a maximum T_C when α approaches 109°; (c) In addition, we find that the Fe–Te bond length is significantly shorter in the solid solution than in the binary $Fe_{1.127}Te$; (d) The results from the *ab initio* calculations based on spin density function theory yielded an optimized structure with distinct z coordinates for Se and Te, in agreement with the experiment. The valence charge distribution in the Fe–Se bonds was found to be different from that in the Fe–Te bonds where the latter pair hybridizes more strongly. Thus, the shorter Fe–Te bond and its stronger hybridization most likely contribute to the enhancement of the local moment that would lead to a magnetic instability.

II. EXPERIMENT

The neutron diffraction measurements were performed using the high intensity powder diffractometer (HIPD) of Los

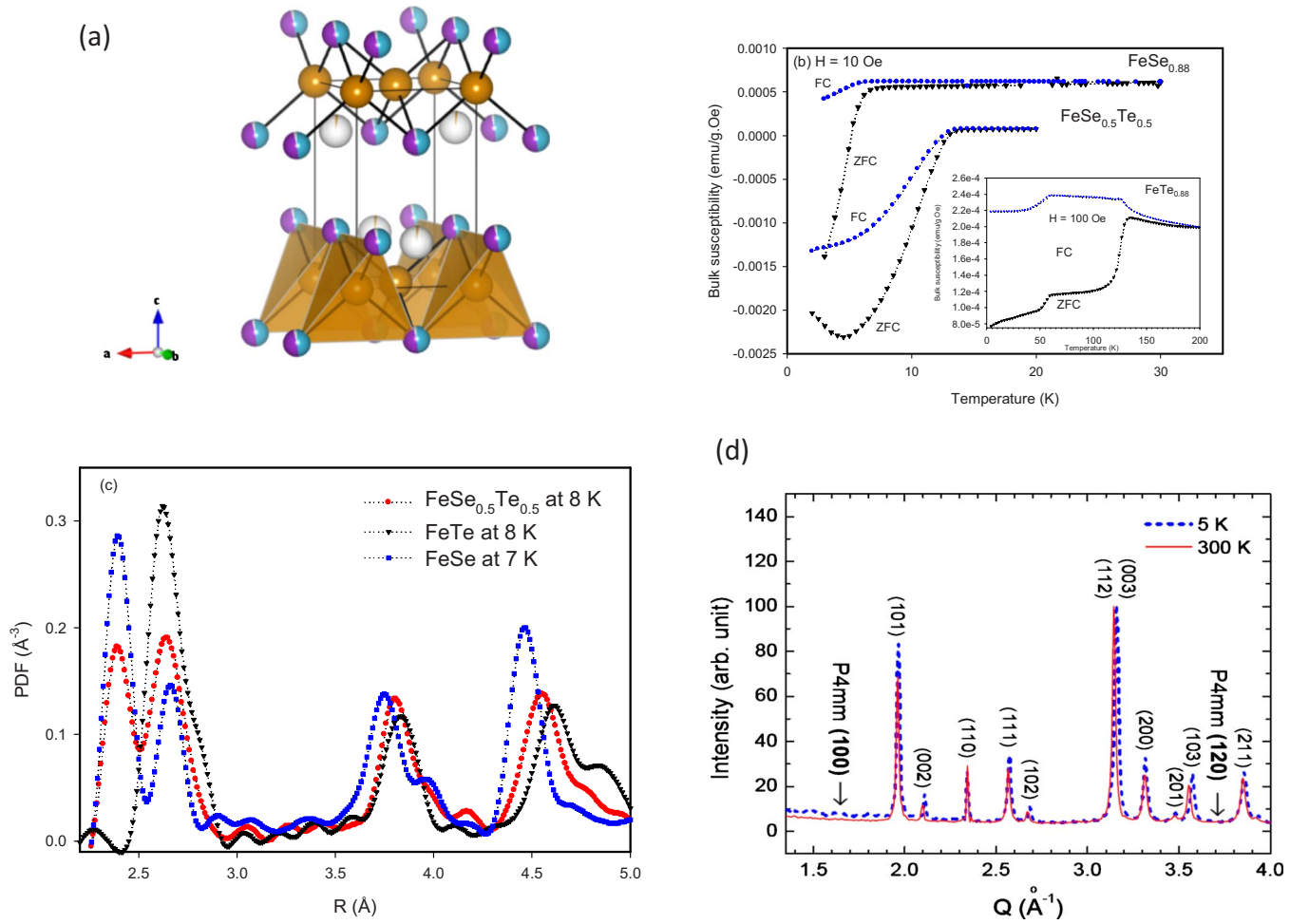

FIG. 1. (Color online) (a) The crystal structure of $FeSe_{1-x}Te_x$ with the $P4/nmm$ symmetry. In this symmetry, the Te and Se ions share the same site. (b) The bulk susceptibility measured at $H=10$ Oe for FeSe and $FeSe_{0.5}Te_{0.5}$. In the inset, data are shown for FeTe at $H=100$ Oe. Our FeTe sample exhibits two transitions due to the presence of an impurity phase, Fe_3O_4, of less than 1 percent: on cooling, the first drop in the bulk susceptibility at 120 K is because of the Verwey transition in Fe_3O_4 while the second drop in the susceptibility is due to the antiferromagnetic transition of FeTe (Ref. 12). (c) The local atomic structure of the three compositions. The pair density function, $\rho(r)=\rho_o+\frac{1}{2\pi^2 r}\int[S(Q)-1]\sin QrdQ$, is plotted. The PDF is multiplied by the coherent neutron scattering length of the different elements ($b_{Se}=7.97$ fm, $b_{Fe}=9.45$ fm, and $b_{Te}=5.80$ fm) and divided by the $\langle b\rangle^2$. The first peak corresponds to the shortest distance in the tetrahedral unit, consisting of Fe-Se or Fe-Te correlations. The second peak corresponds to the second nearest neighbor correlations of Fe-Fe. In FeTe, the first peak has a shoulder to the right as the separation between Fe-Fe and Fe-Te is not well resolved. In FeSe, the Fe–Fe and Fe–Se bond correlations are clearly resolved. In $FeSe_{0.5}Te_{0.5}$, two peaks of comparable intensity are observed. (d) The diffraction patterns of $FeSe_{0.5}Te_{0.5}$ at 300 and 5 K obtained at the Pohang light source using an incident beam of 12 keV are compared. No new Bragg peaks are present with cooling that excludes the possibility of the $P4mm$ symmetry.

Alamos National Laboratory on polycrystalline samples and the data were analyzed using the Rietveld and the PDF techniques to determine the average and local atomic structures of the superconducting FeSe and $FeSe_{0.5}Te_{0.5}$, and of the nonsuperconducting $Fe_{1.127}Te$. FeTe undergoes an antiferromagnetic long-range order below $T_N\sim 60$ K as determined from the bulk magnetic susceptibility data shown in the inset of Fig. 1(b). With the substitution of Te with Se, the Néel order is suppressed and superconductivity emerges with the highest T_C reached at around the $FeSe_{0.5}Te_{0.5}$ concentration [$\sim$13 K in our sample as seen in Fig. 1(b)]. On the other end, FeSe exhibits a T_C of $\sim$7 K [also shown in Fig. 1(b)]. From the time-of-flight pulsed neutron diffraction data the structure function is obtained which is subsequently Fourier transformed to determine the PDF that provides direct information on the interatomic bond distances in real space without the assumption of crystal periodicity.[24] The PDF is a measure of the probability of finding two atoms separated by a distance R (Å) in real space, and for simple systems, it purely follows the symmetry of the unit cell. The crystallographic analysis of these samples has been reported in Refs. 17 and 26. The crystal symmetry for all compounds at temperatures above their respective transitions is tetragonal with the $P4/nmm$ space group. On cooling below the magnetic transition, $Fe_{1.127}Te$ undergoes a structural transition to a monoclinic $P2_1/m$ phase,[12] FeSe is suggested to undergo a transition to an orthorhombic $Cmma$ phase[27] while $FeSe_{0.5}Te_{0.5}$ (Ref. 12) is presumed to remain in the tetragonal phase. The refinement results for all three samples are summarized in Tables I and II. The absence of a structural tran-

TABLE I. Structural properties of FeSe and FeTe1.127. FeSe: refined parameters for *Cmma* space group at 7 K; a=5.324 95(1) Å, b=5.309 03(1) Å, c=5.479 20(9) Å; and R_p=3.43%, wR_p=5.83%. The Se ion concentration is close to 1. $Fe_{1.127}Te$: refined parameters at 70 K (first line) using space group $P4/nmm$; a=3.810 00(8) Å, c=6.245 55(2)Å; and R_p=1.91%, wR_p=3.09%. At 8 K (second line), space group $P2_1/m$; a=3.835 68(5) Å, b=3.785 39(8) Å, c=6.249 08(0) Å, β=90.6286°; and R_p=2.06%, wR_p=4.67%. A second Fe ion is added.

Atom	Site	x	y	z	U (Å^2)	Frac
			FeSe			
Fe	$4a$	$\frac{1}{4}$	0	0	0.0013(5)	1.0
Se	$4g$	0	$\frac{1}{4}$	0.26686(3)	0.0013(6)	1.0
			$Fe_{1.127}Te$			
Fe(1)	$2a$	$\frac{3}{4}$	$\frac{1}{4}$	0	0.0008(4)	1.0
		0.73977(4)	$\frac{1}{4}$	0.00412(6)	0.0006(6)	1.0
Te	$2c$	$\frac{1}{4}$	$\frac{1}{4}$	0.28223(2)	0.0010(1)	1.0
		0.24627(1)	$\frac{1}{4}$	0.28340(3)	0.0004(5)	1.0
Fe(2)	$2c$	$\frac{1}{4}$	$\frac{1}{4}$	0.71426(6)	0.0099(9)	0.1267(7)
		0.27271(7)	$\frac{1}{4}$	0.71675(3)	0.0028(2)	0.1267(7)

sition in the highest T_C material, $FeSe_{0.5}Te_{0.5}$, parallels the observations reported in $LaO_{1-x}F_xFeAs$ (Ref. 1) with F chemical doping that has, in turn, been linked to the suppression of static antiferromagnetic ordering.

III. RESULTS

The results from the Rietveld refinement of all three samples are plotted in Fig. 2(a)–2(c) above and below their respective transition temperatures. The $Fe_{1.127}Te$ and $FeSe_{0.5}Te_{0.5}$ are single phase samples while FeSe contains about 16% of β-Fe_7Se_8, which has the hexagonal NiAs-type structure. Also shown in this figure is a comparison of the high angle detector bank of the diffraction patterns in d spacing at low temperatures [Fig. 2(d)]. This shows that in $FeSe_{0.5}Te_{0.5}$ the peaks are not unusually broad and it is not made of two phases such as a mixture of FeSe and $Fe_{1.127}Te$. The three patterns are different due to their having different symmetries as summarized in Tables I and II, while the shift in the pattern shows how the lattice expands with the addition of Te for Se.

The PDF's corresponding to the local atomic structures show distinct differences among the three compositions [Fig. 1(c)] as well. In $Fe_{1.127}Te$ (black symbols), the peaks are consistently shifted to higher R values because the lattice expands with the larger Te ion. The first tall peak with a shoulder to the right corresponds to Fe–Te and Fe–Fe bond correlations at ~2.62 and 2.82 Å, respectively. In FeSe, on the other hand, the Fe–Se and Fe–Fe bond correlations are better resolved, yielding two peaks at ~2.39 and 2.69 Å, respectively, while the pattern is shifted to the left because of the smaller Se ion. Using the atomic coordinates and unit cell dimensions of the crystallographic structures of Table I, a model PDF is readily calculated using the following expression: $\rho(r)=\frac{1}{4\pi Nr^2}\sum_{ij}\frac{c_ic_jb_ib_j}{\langle b\rangle^2}\delta(r-r_{ij})$, where c_{ij} is the concentration and b_{ij} the scattering length of the elements i and j. For the case of FeSe, a local model calculated from the *Cmma* symmetry[27] yields a good agreement to the experimentally determined PDF at 7 K, although some small differences are observed [Fig. 3(a)]. More importantly, the split of the first peak is reproduced well, indicating that the local periodicity corresponds to that for the average crystal symmetry. Similarly, the local atomic structure corresponding to $Fe_{1.127}Te$ is reproduced well assuming a model based on the average symmetry of $P2_1/m$ at 8 K (Ref. 12) [Fig. 3(b)].

On the other hand, a comparison of the experimental PDF representing the solid solution of $FeSe_{0.5}Te_{0.5}$ to a model PDF calculated based on the reputed tetragonal $P4/nmm$

TABLE II. Refined parameters using space group $P4/nmm$ at 8 K are listed for FeSe0.5Te0; a=3.792 48(5) Å, c=5.940 03(1) Å and R_p=4.22%, wR_p=6.04%. At 16 K (not listed), a=3.792 54(4) Å, c=5.939 82(2) Å and R_p=2.92%, wR_p=4.64%. If a second Fe ion is added, the refinement improves minimally.

Atom	Site	x	y	z	U(Å^2)	Frac
Fe	$2a$	$\frac{3}{4}$	$\frac{1}{4}$	0	0.01091(4)	1.0
Se/Te	$2c$	$\frac{1}{4}$	$\frac{1}{4}$	0.26734(3)	0.01133(8)	1.0

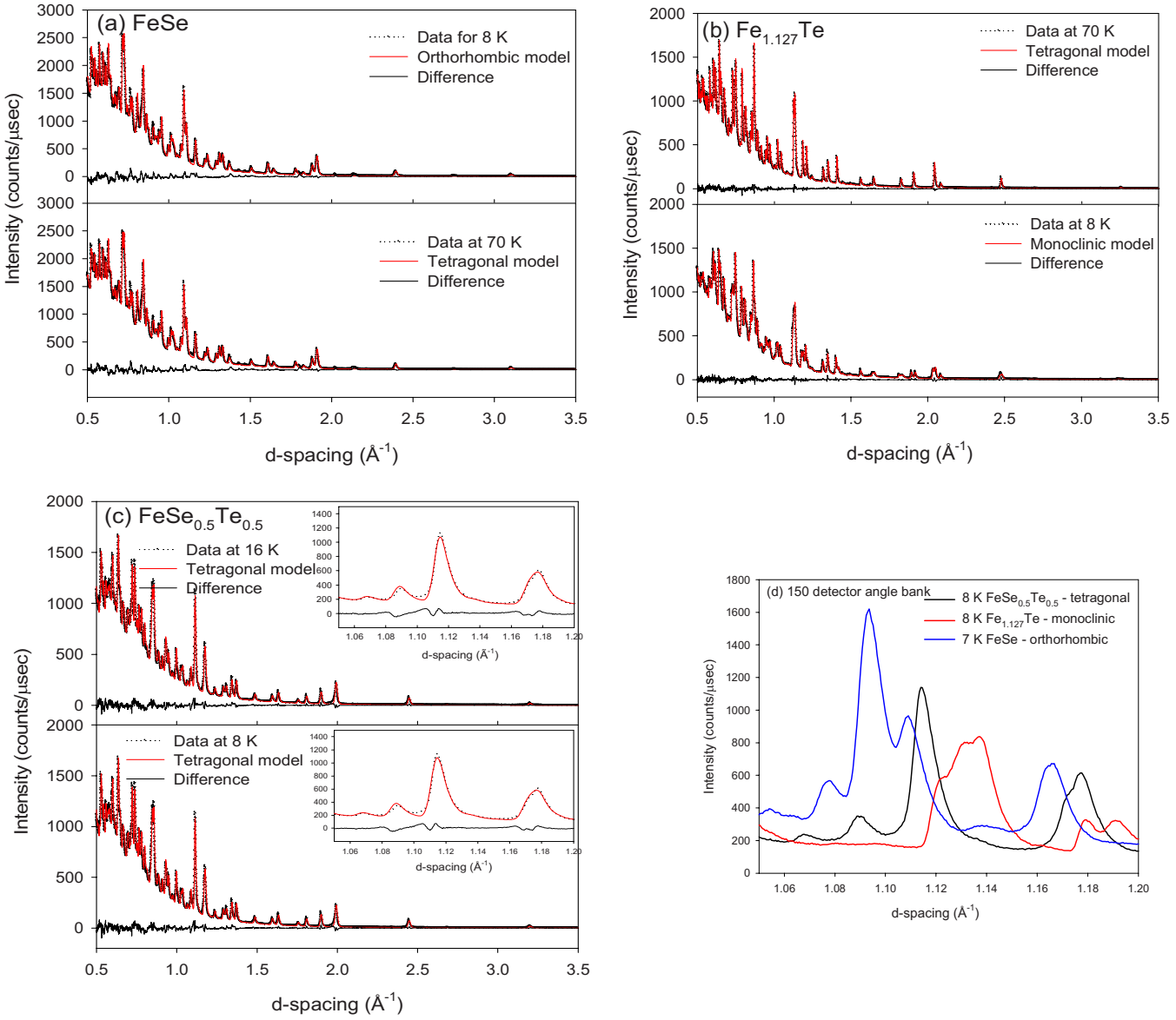

FIG. 2. (Color online) The Rietveld refinement results at two temperatures for (a) FeSe, (b) $Fe_{1.127}Te$, and (c) $FeSe_{0.5}Te_{0.5}$. Also shown in the figures are the differences between observed and calculated patterns. The refinement results are summarized in Tables I and II. In (d), a comparison of the peak widths of the three samples is shown. $FeSe_{0.5}Te_{0.5}$ is not a mixture of FeSe and $Fe_{1.127}Te$. The insets in (c) show an expanded region of the diffraction pattern compared to the model fitting for the $FeSe_{0.5}Te_{0.5}$ compound.

symmetry does not fit well at all, particularly in the short-range structure involving the tetrahedral coordination [blue line in Fig. 4(a) and Table I]. In this symmetry, the Te and Se ions share the same site i.e., same z coordinate of $z=0.2673$. Additionally, it can be seen from Fig. 1(c) that a comparison of the local structure for $FeSe_{0.5}Te_{0.5}$ shows that it does not resemble the one obtained for $Fe_{1.127}Te$ or FeSe, because the first two peaks in $FeSe_{0.5}Te_{0.5}$ are almost evenly split at 2.39 and 2.64 Å with comparable intensities in the solid solution. The agreement factor[25] calculated between this model and the experimental PDF yields a value of $A=0.5093$ from 1.5 to 10 Å. This leads us to question (1) whether or not the Se and Te ions have the same local environment; (2) how the Se and Te ions are distributed in the lattice; and 3) how the local angle α between the ligand and Fe changes with doping from the end members to $FeSe_{0.5}Te_{0.5}$. From the crystallographic refinement, for instance, it is found that α decreases from 104.02° in FeSe to 100.58° in $FeSe_{0.5}Te_{0.5}$.[17]

As long as Te and Se share the same site, it is impossible to reproduce the splitting, thus it is necessary to lower the local symmetry in a way that allows for two distinct Se and Te sites. In this scenario, a local atomic model is built assuming two z coordinates for Se and Te with the parameters listed in Table III, giving rise to two distinct local environments around the Fe ion. In this arrangement, the even split of the peaks is reproduced as seen in Fig. 4(a) (black line). The agreement factor in this case is $A=0.3083$. The partial PDF's shown in Fig. 4(b) are only to demonstrate that the Fe–Se and Fe–Te bond lengths are quite different locally. However, if the high symmetry $P4/nmm$ phase is assumed, there is only one partial function arising from the Fe-Se/Te

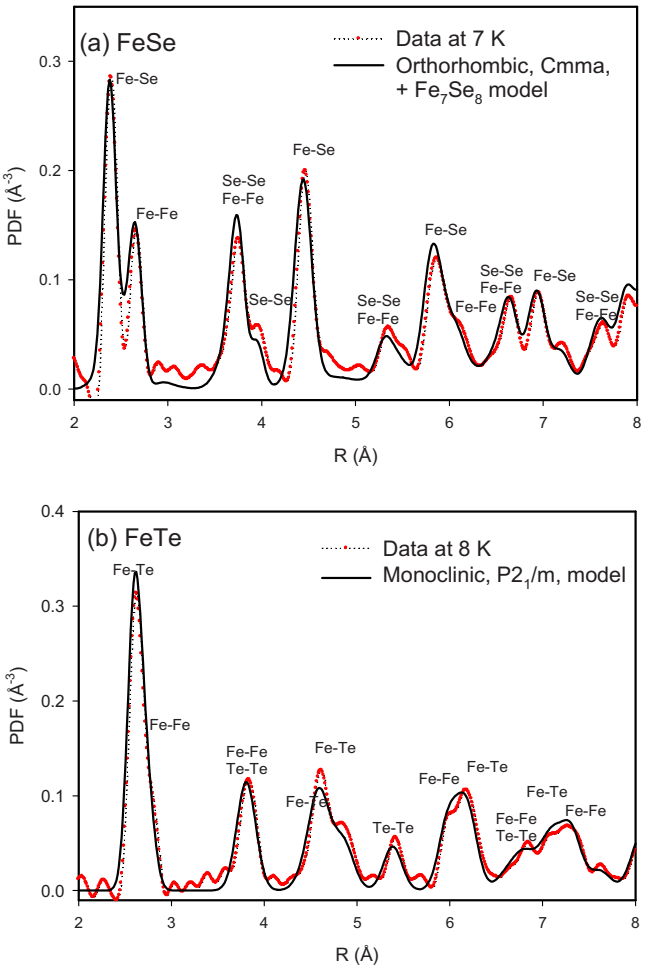

FIG. 3. (Color online) (a) The local atomic structure of FeSe. The red symbols correspond to the experimental PDF determined from the diffraction data and the solid line corresponds to the model calculated from the crystal symmetry. The model consists of 84% of the *Cmma* phase and 16% of the Fe_7Se_8 phase with the $P3_1$ symmetry as determined from the crystallographic refinement results. Even with the second phase added, the fit is not perfect and calls for further investigation of the real local structure of FeSe. (b) The local atomic structure of FeTe. The red symbols correspond to the experimental PDF determined from the diffraction data and the solid line corresponds to the model calculated from the $P2_1/m$ crystal symmetry.

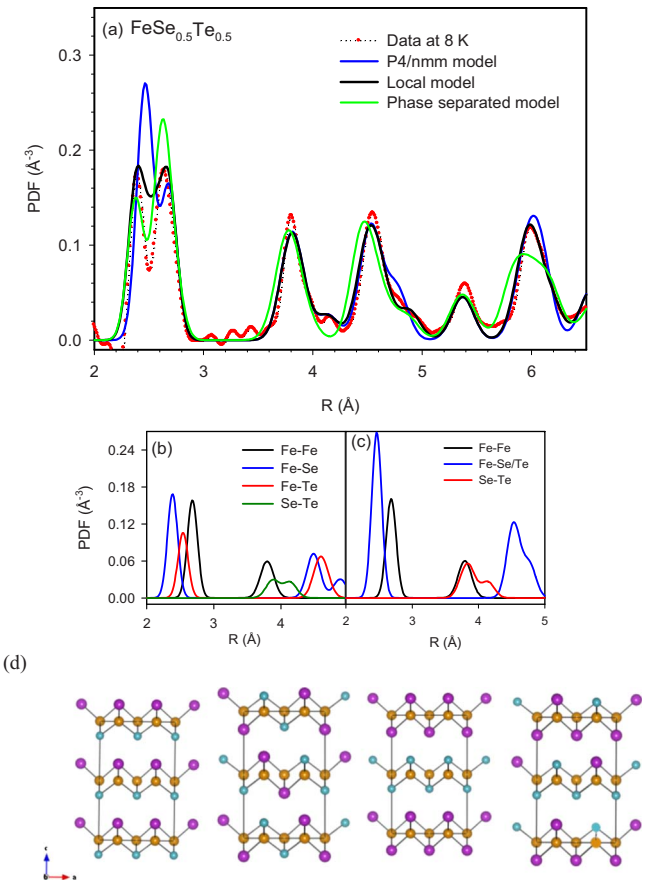

FIG. 4. (Color online) (a) The local atomic structure of $FeSe_{0.5}Te_{0.5}$. The red symbols correspond to the experimental PDF determined from the diffraction data. The blue solid line corresponds to a model calculated from the $P4/nmm$ crystal symmetry. The green solid line corresponds to a model calculated assuming the presence of two separate phases, FeTe in the $P2_1/m$ symmetry and FeSe in the *Cmma* symmetry. The black solid line corresponds to a local structure model assuming two distinct sites for Se and Te using the coordinates listed in Table I. This model provides the best agreement with the experimental data. It yields two types of Te–Fe–Te and Se–Fe–Se bond angles. For distances greater than 3.5 Å, the $P4/nmm$ and local models are comparable, with A=0.2380 for the former and A=0.2193 for the latter. (b) The partial PDF's of the local model that shows the different bond correlations with regard to Fe-Se and Fe-Te. (c) The partial PDF's calculated using the $P4/nmm$ symmetry where only one Fe–Se/Te bond correlation is present. (d) Crystal models representing 4 different arrangements of Se and Te ions. In the first, Se and Te are ordered in layers. In the second, Se and Te alternate in a 2×2 model. In the third, Te and Se tetrahedra are separated. In the fourth model, a 3×1 configuration is adopted.

correlations as shown in Fig. 4(c). For comparison, a phase separated model is also shown (green line) to exclude the possibility of a linear combination of FeSe and FeTe crystal phases. To see how the bond angle α between the chalcogen ions and Fe changes with composition, in FeSe $\alpha=104.02°$ while in FeTe $\alpha=94.09°$. Assuming the $P4/nmm$ crystal symmetry for $FeSe_{0.5}Te_{0.5}$, $\alpha=100.58°$, thus the angle decreases instead of increasing as T_C goes up in $FeSe_{0.5}Te_{0.5}$. However, in the local structure, the angle between Se-Fe-Se increases to 105.20° while the angle between Te-Fe-Te becomes 96.47°. If indeed the Se and Te ions occupy different crystallographic sites as suggested here, the distance between the Fe–Se bonds is 2.39 Å and between the Fe–Te bonds is 2.55 Å, which is actually shorter than the Fe–Te bond length in the binary FeTe sample, while the Fe-Se distance is the same as in the binary.

As the Se and Te ions occupy distinct lattice sites, it is natural to wonder how they are organized and whether or not they order in some fashion. If Se and Te ordering were possible as shown in the first crystal model of Fig. 4(d), the $P4mm$ space group, a subgroup of $P4/nmm$, would have been appropriate to describe their arrangement in real space. The refinement results for the $P4mm$ phase are summarized

TABLE III. Parameters for the local structure model at 8 K for $FeSe_{0.5}Te_{0.5}$. The lattice constants are set at $a=b=3.8003$ and $c=5.9540$ Å. The z coordinates of Se and Te are different from those determined using the $P4/nmm$ symmetry, thus the site symmetry is lowered. In $P4/nmm$ symmetry, the Se and Te ions share the same site at $z=0.26734$.

Atom	x	y	z	Frac.
Fe(1)	$\frac{1}{2}$	0	0	1.0
Fe(2)	0	$\frac{1}{2}$	0	1.0
Se	0	0	0.756	1.0
Te	$\frac{1}{2}$	$\frac{1}{2}$	0.285	1.0

in Table IV. However, our synchrotron results obtained at the Pohang Light Source at the 11A beamline and shown in Fig. 1(d) from a crushed single crystal demonstrate that no new superlattice peaks appear with cooling down to 5 K, as would have been expected from anion ordering. Hence, the Se and Te atoms are randomly arranged in the crystal lattice, where a combination of different organizations of the Se and Te ions as shown in Fig. 4(d), while always preserving two distinct z coordinates for Se and Te, is most likely present.

To further examine whether or not the estimated difference in the z coordinates of Se and Te is reasonable, we performed *ab initio* structure optimization for the first crystal model in Fig. 4(d) using the Tokyo AB INITIO Program Package.[28] The choice of model is irrelevant as the actual position of the Se and Te ions in the lattice does not play a role but rather, their chemical nature is important. Four kinds of magnetic order were assumed: paramagnetic, G-type antiferromagnetic (AF), stripe-type AF, and double stripe-type AF structures. The generalized gradient approximation (GGA) exchange-correlation functional plane-wave basis set[29] and the ultrasoft pseudopotentials[30] in the Kleinman-Bylander representation[31] were used. The energy cutoffs in wave function and charge density were set to 64 and 900 Ry, respectively. From Table V(a) it can be seen that (1) the stripe AF structure is the most stable, (2) the magnetic moment is as large as 2 μ_B for all AF structures, and (3) the z coordinates for Se and Te are underestimated for the paramagnetic solution, while there is a nice agreement between the experimental and theoretical results for the AF solutions. The large ordered moment is common with the use of LDA in many iron-based superconductors,[2,32] namely, it has been known that structure optimization works successfully if AF order is assumed even though no AF order is present. Thus we may conclude that the difference in the z coordinates of Se and Te estimated in the experiment is reasonable.

Additionally, maximally localized Wannier functions (MLWFs)[33] were constructed to study the valence-charge distribution in the Fe-Se-Te layers. For the experimental structure of Table III, we first obtained the band dispersion for the paramagnetic solution and made MLWFs from ten bands around the Fermi level (which have the Fe-3d character). We then calculated the center of gravity of the MLWFs with the results listed in Table V(b). For FeSe or $Fe_{1.127}Te$, the center of gravity of each MLWF resides at the Fe site. However, for $FeSe_{0.5}Te_{0.5}$, it shifts toward the Te layer, which suggests that the hybridization between Fe and Te is stronger than that between Fe and Se, and the MLWFs have a long tail in the direction of the Fe–Te bonds. Thus, in $FeSe_{0.5}Te_{0.5}$, the valence charge distribution in Fe-Se bonds and Fe–Te bonds are expected to be different. Note that the use of the ordered model as a starting point in the calculation is not the origin of the difference in the hybridization between Fe and Te/Se. The main reason for this is the difference in the chemical nature of Se and Te, and their ordering has nothing to do with the hybridization between Se/Te and Fe. At the same time, in the structure optimization, the chalcogen z coordinates come out to be different, just as in the experiment, which is unrelated to their ordering scheme. Indeed, the most significant issue is not that Se and Te occupy different sites but that they have different z coordinates.

IV. DISCUSSION

From this local structure study, we have extracted the actual bond lengths and bond angles which are in turn significant in understanding how the band structure and in particular the Fermi surface change with doping. While it is generally the case that the general features of the band structure are essentially captured by simply using the average structure, this cannot be sufficient to explain why certain bands cross the Fermi surface. In this paper, we have shown that the average structure of the $FeSe_{0.5}Te_{0.5}$ in this binary superconductor does not accurately represent the bond length and bond angles between Fe and the two chalcogens. In an analogous way to hydrostatic pressure, the substitution of the larger Te ion for the smaller Se results in internal chemical pressure. However, on average, the bond angle between Fe and the chalcogens decreases, instead of getting close to 109°. Therefore, why does T_C go up in this system? We made the following distinct observations such as: (1) the Fe-Te bond length is much shorter than in the binary $Fe_{1.127}Te$ while the bond angle is actually larger in the solid solution, in contrast to the crystallographic refinement; (2) the Fe–Se bond length in $FeSe_{0.5}Te_{0.5}$ is about the same as in

TABLE IV. Refined parameters using space group $P4mm$ at 8 K; $a=3.79264(9)$ Å, $c=5.94038(1)$ Å and $R_p=3.69\%$, $wR_p=5.36\%$.

Atom	Site	x	y	z	U(Å^2)	Frac
Fe	2a	$\frac{1}{2}$	0	0	0.0029(6)	1.0
Se	1a	0	0	0.7534(2)	0.0004(7)	1.0
Te	1b	$\frac{1}{2}$	$\frac{1}{2}$	0.2916(4)	0.0022(9)	1.0

TABLE V. (a) Total energy of each AFM state in reference to that of the paramagnetic (PM) state in units of meV/formula (ΔE), magnetic moment of Fe in units of μ_B (M), and internal coordinates associated with anion height from the Fe layer ($z_{Se/Te}$) obtained by structural optimization. (b) Displacements of the center of the Wannier function localized at Fe(1) and Fe(2) sites, where the z values from the Fe plane ($z=0$) are shown in the unit of a.u. The largest shift is observed for the d_{yz} orbital of Fe(1) and the d_{zx} one of Fe(2) which are the ones that hybridized most strongly with the Te p orbitals.

(a)	ΔE	M	z_{Se}	z_{Te}
PM	0		−0.2242(1.334 Å)	0.2744(1.633 Å)
G-type AFM	−147.54	2.14	−0.2453(1.460 Å)	0.2906(1.730 Å)
Stripe AFM	−198.61	2.30	−0.2460(1.474 Å)	0.2925(1.741 Å)
Double-stripe AFM	−174.19	2.45	−0.2564(1.526 Å)	0.3003(1.78 Å)

(b) MLWF	⟨Fe(1)⟩(a.u.)	⟨Fe(2)⟩(a.u.)
	z	
d_{xy}	0.057188529540	0.057190958975
d_{yz}	0.179277684686	0.043166144631
d_{z^2}	0.057672527487	0.057701642460
d_{zx}	0.04315708064	0.179291217237
d_{x^2}	0.092899952649	0.092953036438

the binary FeSe, although the bond angle increases as well. These effects cannot be described by a simple substitution of Te for Se. One can think of the role of Te as if it effectively dopes the system, supported by the stronger hybridization it exhibits with Fe. The off-centering of the Wannier orbitals of Fe occurs when directed toward Te, and not so with Se, and should be understood as an effect purely due to the different chemical nature of the two ions and not due to their ordering nature in the crystal structure. The local information provided in this paper has direct implications on the charge transfer mechanism between the chalcogen layer and the Fe layer. It can also be inferred from the results of this work that the effective local moment around Fe will be directly affected by the local environment.

How does the difference in the hybridization affects the pairing instability? As presented in Ref. 34, the occupation number of each orbital is different for Fe-Se and Fe-Te. In that sense, the change in the hybridization between Fe-3d and Te/Se-p would work as effective doping. At the same time, the peak splitting in the density of states (DOS), which is caused by the hybridization of x^2-y^2 is much smaller in FeTe. This means that FeTe tends to have a larger magnetic moment. Replacing Se with Te will enhance the formation of the local moment, which will lead to the magnetic instability. If the superconductivity is mediated by spin fluctuation, the change in the hybridization indeed must affect the superconductivity.

The calculations predict a particular stability for stripe antiferromagnetism with a large ordered moment. However, experiments predict at best short-range magnetic order in samples with $T_C \sim 14$ K . Indeed, LDA gives a larger ordered moment, while the system does not have long-range order in reality. This is a very well-known problem of LDA for iron pnictides. The size of the local moment is large, but it fluctuates so quickly, so that the ordered moment is severely suppressed. Calculations of $\chi(t)=\langle S(0)S(t)\rangle$ by means of LDA+DMFT (DMFT=dynamical mean field theory, which can treat dynamical quantities, in contrast with LDA, which is a static mean field theory) would shed light on this issue.

In summary, using neutron and x-ray scattering measurements on polycrystalline samples of the $FeSe_{1-x}Te_x$ system and *ab initio* structure optimization, we determined that the local structures around Te and Se are distinctly different, reducing the crystal symmetry, and with direct implications on the hybridization with Fe and the charge distribution. It is possible that replacing Se with Te will enhance the formation of the local moment, which will lead to magnetic instability.[34] If the superconductivity is mediated by spin fluctuation, the change in the hybridization indeed affects the superconductivity.

ACKNOWLEDGMENTS

We thank Z. Tesanovic and M. Norman for helpful discussions. This work is supported by the U.S. Department of Energy, Division of Materials Science under Grant No. DE-FG02–01ER45927 and the Los Alamos National Laboratory is operated by the Los Alamos National Security LLC.

[1] C. De la Cruz, Q. Huang, J. W. Lynn, Jiying Li, W. Ratcliff, II, J. L. Zarestky, H. A. Mook, G. F. Chen, J. L. Luo, N. L. Wang, and Pengcheng Dai, Nature (London) **453**, 899 (2008).
[2] I. I. Mazin, D. J. Singh, M. D. Johannes, and M. H. Du, Phys. Rev. Lett. **101**, 057003 (2008).
[3] R. H. Liu, T. Wu, G. Wu, H. Chen, X. F. Wang, Y. L. Xie, J. J. Ying, Y. J. Yan, Q. J. Li, B. C. Shi, W. S. Chu, Z. Y. Wu, and X. H. Chen, Nature (London) **459**, 64 (2009).
[4] A. V. Chubukov, M. G. Vavilov, and A. B. Vorontsov, Phys. Rev. B **80**, 140515(R) (2009).
[5] Y. Kamihara, T. Watanabe, M. Hirano, and H. Hosono, J. Am. Chem. Soc. **130**, 3296 (2008).
[6] D. J. Singh and M.-H. Du, Phys. Rev. Lett. **100**, 237003 (2008).
[7] T. Yildirim, arXiv:0902.3462 (unpublished).
[8] A. Subedi, L. Zhang, D. J. Singh, and M.-H. Du, Phys. Rev. B **78**, 134514 (2008).
[9] M. H. Fang, H. M. Pham, B. Qian, T. J. Liu, E. K. Vehstedt, Y. Liu, L. Spinu, and Z. Q. Mao, Phys. Rev. B **78**, 224503 (2008).
[10] K. Yeh, T. Huang, Y. Huang, T. Chen, F. Hsu, P. Wu, Y. Lee, Y. Chu, C. Chen, J. Luo, D. Yan, and M. Wu, Europhys. Lett. **84**, 37002 (2008).
[11] Z. A. Ren, Wu Yue-Qin, and Zhang Li-Chun, Chin. Phys. Lett. **25**, 2385 (2008).
[12] W. Bao *et al.*, Phys. Rev. Lett. **102**, 247001 (2009).
[13] S. Li, C. de la Cruz, Q. Huang, Y. Chen, J. W. Lynn, Jiangping Hu, Fong-Chi Hsu, Kuo-Wei Yeh, Maw-Kuen Wu, and Pengcheng Dai, Phys. Rev. B **79**, 054503 (2009).
[14] T. Imai, K. Ahilan, F. L. Ning, T. M. McQueen, and R. J. Cava, Phys. Rev. Lett. **102**, 177005 (2009).
[15] X. H. Chen, T. Wu, G. Wu, R. H. Liu, H. Chen, and D. F. Fang, Nature (London) **453**, 761 (2008).
[16] D. Reznik, K. Lokshin, D. Mitchell, D. Parshall, W. Dmowski, D. Lamago, R. Heid, K. Bohnen, A. Sefat, M. Mcguire, B. Sales, D. Mandrus, A. Asubedi, D. Singh, A. Alatas, M. Upton, A. Said, Y. Shvydko, and T. Egami, Phys. Rev. B **80**, 214534 (2009).
[17] K. Horigane, Nao Takeshita, Chul-Ho Lee, Haruhiro Hiraka, and Kazuyoshi Yamada, J. Phys. Soc. Jpn. **78**, 063705 (2009).
[18] A. Kreyssig, M. A. Green, Y. Lee, G. D. Samolyuk, P. Zajdel, J. W. Lynn, S. L. Bud'ko, M. S. Torikachvili, N. Ni, S. Nandi, J. B. Leão, S. J. Poulton, D. N. Argyriou, B. N. Harmon, R. J. McQueeney, P. C. Canfield, and A. I. Goldman, Phys. Rev. B **78**, 184517 (2008).
[19] V. Cvetkovic and Z. Tesanovic, EPL **85**, 37002 (2009).
[20] V. Sidorov, A. Tsvyashchenko, and R. Sadykov, arXiv:0903.2873 (unpublished).
[21] F. C. Hsu, J.-Y. Luo, K.-W. Yeh, T.-K. Chen, T.-W. Huang, P. M. Wu, Y.-C. Lee, Y.-L. Huang, Y.-Y. Chu, D.-C. Yan, and M.-K. Wu, Proc. Natl. Acad. Sci. U.S.A. **105**, 14262 (2008).
[22] T. M. McQueen, Q. Huang, V. Ksenofontov, C. Felser, Q. Xu, H. Zandbergen, Y. S. Hor, J. Allred, A. J. Williams, D. Qu, J. Checkelsky, N. P. Ong, and R. J. Cava, Phys. Rev. B **79**, 014522 (2009).
[23] V. B. Zabolotnyy, D. S. Inosov, D. V. Evtushinsky, A. Koitzsch1, A. A. Kordyuk, G. L. Sun, J. T. Park, D. Haug, V. Hinkov, A. V. Boris, C. T. Lin, M. Knupfer, A. N. Yaresko, B. Büchner, A. Varykhalov, R. Follath, and S. V. Borisenko, Nature (London) **457**, 569 (2009).
[24] T. Egami and S. J. L. Billinge, *Underneath the Bragg Peaks* (Pergamon Materials Series, Burlington, MA, 2003), Vol. 7.
[25] D. Louca and T. Egami, Phys. Rev. B **59**, 6193 (1999).
[26] K. Horigane, H. Hiraka, and K. Ohoyama, J. Phys. Soc. Jpn. **78**, 074718 (2009).
[27] S. Margadonna, Y. Takabayashi, M. T. McDonald, K. Kasperkiewicz, Y. Mizuguchi, Y. Takano, A. N. Fitch, E. Suard, and K. Prassides, Chem. Commun. **2008**, 5607.
[28] J. Yamauchi, M. Tsukada, S. Watanabe, and O. Sugino, Phys. Rev. B **54**, 5586 (1996).
[29] J. P. Perdew, K. Burke, and M. Ernzerhof, Phys. Rev. Lett. **77**, 3865 (1996).
[30] D. Vanderbilt, Phys. Rev. B **41**, 7892 (1990).
[31] L. Kleinman and D. M. Bylander, Phys. Rev. Lett. **48**, 1425 (1982).
[32] I. I. Mazin, M. D. Johannes, L. Boeri, K. Koepernik, and D. J. Singh, Phys. Rev. B **78**, 085104 (2008).
[33] N. Marzari and D. Vanderbilt, Phys. Rev. B **56**, 12847 (1997).
[34] T. Miyake, K. Nakamura, R. Arita, and M. Imada, J. Phys. Soc. Jpn. **79**, 044705 (2010).